Few-Mode Superposition for High-Efficiency Generation of Tailored Partially Coherent Light

Wang, Zhuoyi; Lu, Xingyuan; Zhang, Hao; Zhu, Junan; Lu, Xiaotan; Shao, Yifeng; Urbach, H. Paul; Zhan, Qiwen; Cai, Yangjian; Zhao, Chengliang

DOI
10.1021/acsphotonics.4c02613

Publication date
2025

Document Version
Final published version

Published in
ACS Photonics

ACS Photonics

pubs.acs.org/journal/apchd5

Article

Few-Mode Superposition for High-Efficiency Generation of Tailored Partially Coherent Light

Zhuoyi Wang, Xingyuan Lu,* Hao Zhang, Junan Zhu, Xiaotan Lu, Yifeng Shao, H. Paul Urbach, Qiwen Zhan, Yangjian Cai, and Chengliang Zhao*

Cite This: *ACS Photonics* 2025, 12, 2160−2168

Read Online

ACCESS | Metrics & More | Article Recommendations | Supporting Information

ABSTRACT: Partially coherent light is essential in lithography systems, where it improves illumination homogenization, enhances resolution, and mitigates speckle noise, playing a key role in advanced imaging applications. However, efficiently generating and computing partially coherent beams (PCBs) remains a challenge, particularly in high-precision lithography where computational efficiency is critical. Here, we introduce a novel modal-superposition method for PCB synthesis, termed "few-mode superposition" and demonstrate its effectiveness in achieving PCBs with higher precision and efficiency. The method requires significantly fewer modes compared to conventional techniques while maintaining high accuracy in intensity and coherence. We apply the few-mode superposition method to the efficient generation of partially coherent light sources and computational lithography, showcasing its ability to rapidly produce PCBs with nonconventional cross-spectral density functions. This facilitates fast lithography simulations and other applications involving partially coherent light. Our approach significantly accelerates both the generation and calculation of PCBs and holds promise for integration with on-chip laser sources, as well as for high-energy laser generation and lithographic mask design.

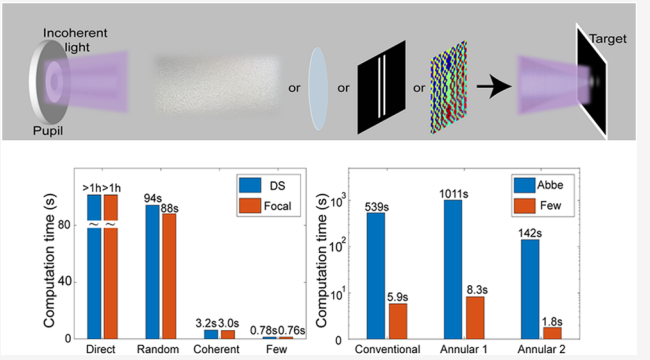

KEYWORDS: *partially coherent light, modal superposition, efficient generation, computational imaging*

1. INTRODUCTION

With the development of conventional and structured lasers,[1−3] high-coherence light sources have found widespread applications. However, decoherence is ubiquitous and often occurs in complex media or randomly fluctuating light fields. Counterintuitively, in some scenarios, the decoherence effect can have positive impacts.[3−6] For example, partially coherent beams (PCBs) can enhance computing parallelism without significantly sacrificing accuracy, potentially enabling larger-size photonic tensor cores.[7] By reducing the coherence of the light source, the speckle effect during imaging can be weakened.[8−10] Adjusting the coherent structure of the PCB has further enhanced the beam's shaping capabilities and mitigated the effects of atmospheric turbulence.[11] Recently, PCBs have been utilized for information encoding during propagation through complex media.[12] Nevertheless, decoherence has introduced significant challenges to the numerical calculation of light wave propagation. Treating PCBs in applications such as lithography, high-energy lasers, or synchrotron radiation as fully coherent beams without appropriate corrections can lead to various issues.[13−19]

Based on optical coherence theory,[20] PCBs can be characterized by the cross-spectral density (CSD) function in the space-frequency domain or the mutual coherence function in the space-time domain.[20−22] Since the CSD function contains information about field correlations at two points, it typically involves four-dimensional integral calculations in the analysis of the propagation, imaging, and scattering of partially coherent light beams.[23−26] This renders the analysis of partially coherent beams more time-consuming compared to that of coherent beams. Therefore, incoherent modal-superposition methods, such as coherent-mode, pseudomode, and random-mode superposition,[27,28] have been proposed for representing PCBs and are widely used in imaging and free-space optical communication systems. These methods offer significant advantages in simplifying analysis and reducing time-consumption in integral calculations.[26,29,30] Additionally, incoherent modal-superposition has been employed in the experimental generation of various PCBs.[31−36] Coherent-mode superposition provides critical insights into the global coherence of the source through its weight distribution and

Received: December 31, 2024
Revised: March 12, 2025
Accepted: March 12, 2025
Published: March 18, 2025

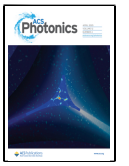

https://doi.org/10.1021/acsphotonics.4c02613
ACS Photonics 2025, 12, 2160−2168

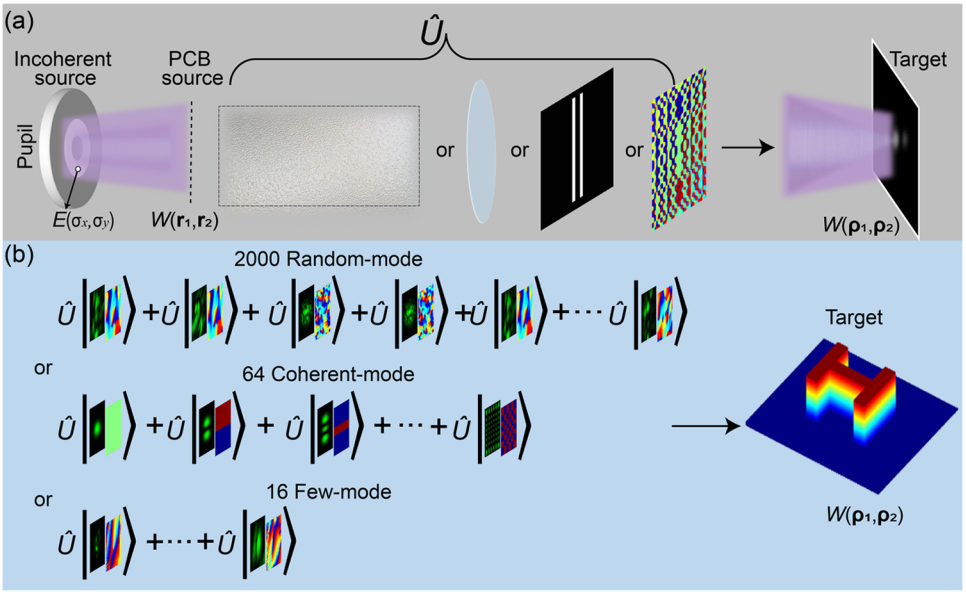

Figure 1. Schematic diagrams of systems with partially coherent beams. (a) Partially coherent light propagates to the target plane through various optical elements. PCB, partially coherent beam. (b) The modal-decomposition methods used to simplify the propagation and imaging calculations with partially coherent illumination.

reveals the local structure of spatial field correlations between pairs of points.[12] However, coherent-mode superposition is suited for simple PCB models, such as Gaussian Schell-mode (GSM) beams and twisted GSM beams. In contrast, pseudomode and random-mode superposition offer greater flexibility and have been utilized for the experimental generation and calculation of more complex PCBs. They can also yield local structures of spatial field correlations at pairs of points, and the coherent modes can be calculated from random modes using orthogonal decomposition.[12] However, the increase in the number of modes results in longer generation and computation times,[27,37,38] hindering real-time generation of PCBs.

To address this problem, we propose a novel incoherent modal-superposition method called few-mode superposition for highly efficiently synthesizing PCBs. By employing the iterative method, fewer modes are required to represent PCBs in terms of the intensity and CSD distributions through various optical elements. The feasibility of generating PCBs using the few-mode superposition method was validated through theoretical analysis, numerical simulations, and experiments. The transmission characteristics of the generated PCBs were confirmed through double-slit interference. The results indicate that the number of modes required to generate PCBs using few-mode superposition is approximately 100 times fewer than that needed with random-mode superposition. Additionally, few-mode superposition can generate PCBs with special correlation functions, which were further utilized in imaging simulations of lithography with various incoherent light sources. Subsequently, the calculation times for the conventional Abbe method and few-mode superposition were compared, with the latter being nearly 100 times faster than the former.

2. THEORY

Without loss of generality, we consider an annular spatially incoherent light source (Figure 1a), in which point light sources illuminate the optical element (e.g., free space, lens, double slits, phase masks) from various angles. Due to the narrow bandwidth of the illumination and the compact optical system, temporal coherence is not considered in the subsequent analysis. For conventional calculations, the imaging results with a monochromatic incoherent light source are obtained by integrating the intensity from each point source,[26] denoted as

$$I_{\text{total}} = \frac{1}{S_{\text{sum}}} \sum_{\sigma_x} \sum_{\sigma_y} S(\sigma_x, \sigma_y) |\widehat{U_0} E(\sigma_x, \sigma_y)|^2 \tag{1}$$

where $S(\sigma_x, \sigma_y)$ is the intensity distribution of incoherent source and S_{sum} is a normalization factor. $\widehat{U_0}$ represents the transmission operator from the pupil plane to the target plane. E represents the electric field at the point (σ_x, σ_y) on the incoherent source plane.

The light emitted by a point light source can be treated as a fully coherent mode. According to the Van Cittert–Zernike theorem, an incoherent light source will transform into a PCB during propagation[20] (PCB source plane in Figure 1a). Then, according to the Hopkins imaging equations,[26] the propagation calculation of PCBs can be expedited using the CSD function, expressed as

$$W(\boldsymbol{\rho}_1, \boldsymbol{\rho}_2) = \hat{U} W(\mathbf{r}_1, \mathbf{r}_2) \tag{2}$$

where $W(\boldsymbol{\rho}_1, \boldsymbol{\rho}_2)$ and $W(\mathbf{r}_1, \mathbf{r}_2)$ represent the CSD function. $\boldsymbol{\rho}$ and $\mathbf{r}$ represent the coordinates on the target plane and the PCB source plane, respectively. $\hat{U}$ represents the transmission operator from the PCB plane to the target plane. Based on Mercer's theorem,[28,39] the CSD function on the PCB source plane and target plane can be decomposed as

$$W(\mathbf{r}_1, \mathbf{r}_2) = \sum_{m=1}^{\infty} \lambda_m \varnothing_m^*(\mathbf{r}_1) \varnothing_m(\mathbf{r}_2) \tag{3}$$

$$W(\boldsymbol{\rho}_1, \boldsymbol{\rho}_2) = \sum_{m=1}^{\infty} \lambda_m [\hat{U}\varnothing_m^*(\mathbf{r}_1)][\hat{U}\varnothing_m(\mathbf{r}_2)] \tag{4}$$

https://doi.org/10.1021/acsphotonics.4c02613
ACS Photonics 2025, 12, 2160−2168

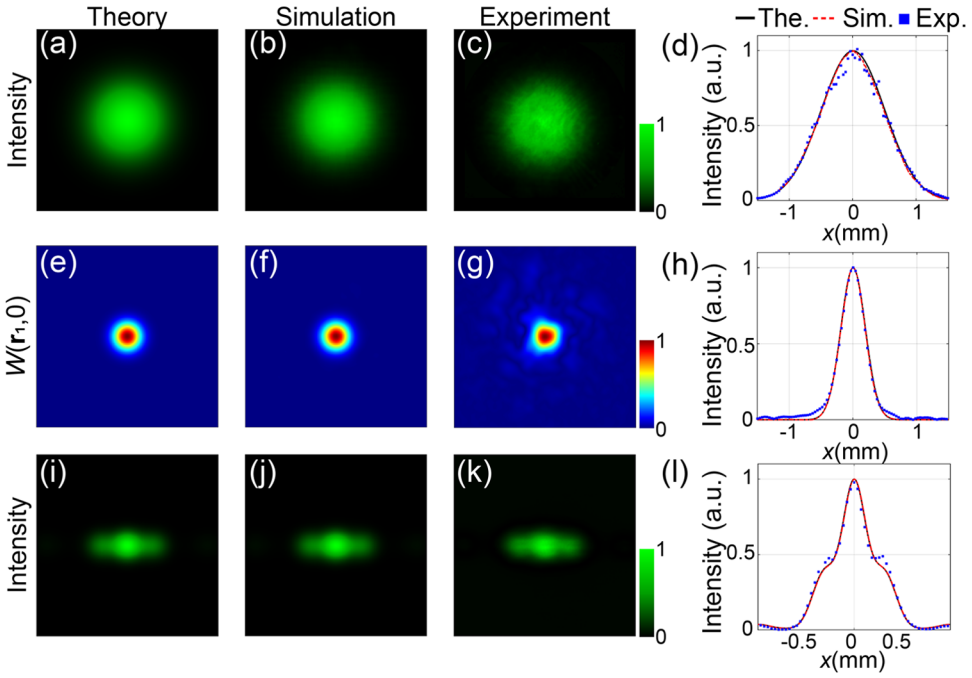

Figure 2. Generation results of the PCB source intensities, CSD amplitude distributions and double-slit interference patterns with few-mode superposition method. (a) represents the theoretical intensity of a GSM beam on the source plane. (b) represents the simulated intensity synthesized by few-mode superposition method and (c) is the corresponding experimental intensity. (e−g) are the theoretical, simulated, and experimental CSD functions on the source plane, respectively. (i−k) Interference patterns on the focal plane after the GSM beam passes through the double-slit. (d, h and l) represent the fitting results of the theory, numerical simulation, and experiment, respectively.

λ_m means the mode weight of the modes. As shown in Figure 1b, the distinction between coherent-mode and random-mode superposition lies in the types of $\varnothing_m(\mathbf{r})$.[28] The coherent-mode and its mode weight are calculated by orthogonal decomposition with a chosen basis. The random-mode is calculated by Fourier transformation of an incoherent light field constructed with plenty of random phases.[28] By using the coherent-mode or random-mode as decomposition basis, the error can only be reduced by deleting some terms. It is not flexible and it lacks feedback in the process.

In comparison, the principle of decomposing partially coherent light into few-mode superposition is achieved through an iterative process (see Methods section for further details). At the source plane, partially coherent light is decomposed into a series of incoherent superpositions of coherent modes, written as $W(\mathbf{r}_1, \mathbf{r}_2) = \sum_{m=1}^{\infty} E_m^*(\mathbf{r}_1)E_m(\mathbf{r}_2)$. Then, the focal intensity of the partially coherent light after passing through a scatterer with a known transmittance function is denoted as I_c. By minimizing the difference between the theoretical intensity I_c and the calculated intensity with a series of modes $E_m(\mathbf{r})$, that is $\min \|I_c - \sum_{m=1}^{M} \mathcal{F}|E_m(\mathbf{r})O(\mathbf{r})|^2\|$ few-mode can be obtained within the preset error range. The minimization is realized by the multiprobe ptychography iterative eigen.[24] Here, "m" denotes the m-th mode, with a total number of M. $\mathcal{F}$ denotes the Fourier transform, and $O(\mathbf{r})$ is the transmittance function of the scatterer. Owing to this design with a feedback mechanism, the few-modes superposition method shows a lower error with the same number of modes and requires fewer modes under the same preset error conditions. As shown in Figure 1b, the results indicate that the number of modes required for the few-mode superposition to synthesize the GSM beam illumination and imaging process is significantly fewer than that required for coherent-mode and random-mode superpositions.

3. RESULT

3.1. Generating PCBs with Few-Mode Superposition.

To demonstrate the feasibility of few-mode superposition method, a GSM beam is used as an example, and the CSD function at the source plane ($z = 0$) is expressed as[40]

$$W(\mathbf{r}_1, \mathbf{r}_2) = A_0 \exp\left(-\frac{\mathbf{r}_1^2 + \mathbf{r}_2^2}{4\sigma_0^2} - \frac{|\mathbf{r}_2 - \mathbf{r}_1|^2}{2\delta_0^2}\right) \quad (5)$$

A_0 is a constant, which was set as 1 in the following analysis. σ_0 and δ_0 are the beam width and the coherence width. Figure 2a,e represents the theoretical intensity (i.e., $I(\mathbf{r}_1) = W(\mathbf{r}_1, \mathbf{r}_2 = \mathbf{r}_1)$[28]) and CSD distribution (with central reference, i.e., $W(\mathbf{r}_1,0)$), respectively. Both are Gaussian distributed, and the waists are determined by σ_0 and δ_0. Here, $\lambda = 532$ nm, $\sigma_0 = 0.5$ mm, and $\delta_0 = 0.2$ mm. Subsequently, few-mode superposition was employed to generate the GSM beam, with the results for intensity and CSD distribution presented in Figure 2b,f. In the experiment, a spatial light modulator was utilized to load holograms generated using few-mode superposition (see Methods section for further details). Figure 2c shows the experimental results for the intensity distribution on the source plane. As the camera cannot directly measure the CSD function, the interference method[41] was employed to measure the CSD distribution, as illustrated in Figure 2g. The background noise is attributed to experimental noise. The fitting curves for intensity and CSD distribution are presented in Figure 2d,h. The results from both numerical simulations and experiments align closely with the theoretical patterns. Additionally, the transmission characteristics of PCBs through a double-slit were analyzed. The slit width is 0.2 mm, and the

https://doi.org/10.1021/acsphotonics.4c02613
ACS Photonics 2025, 12, 2160−2168

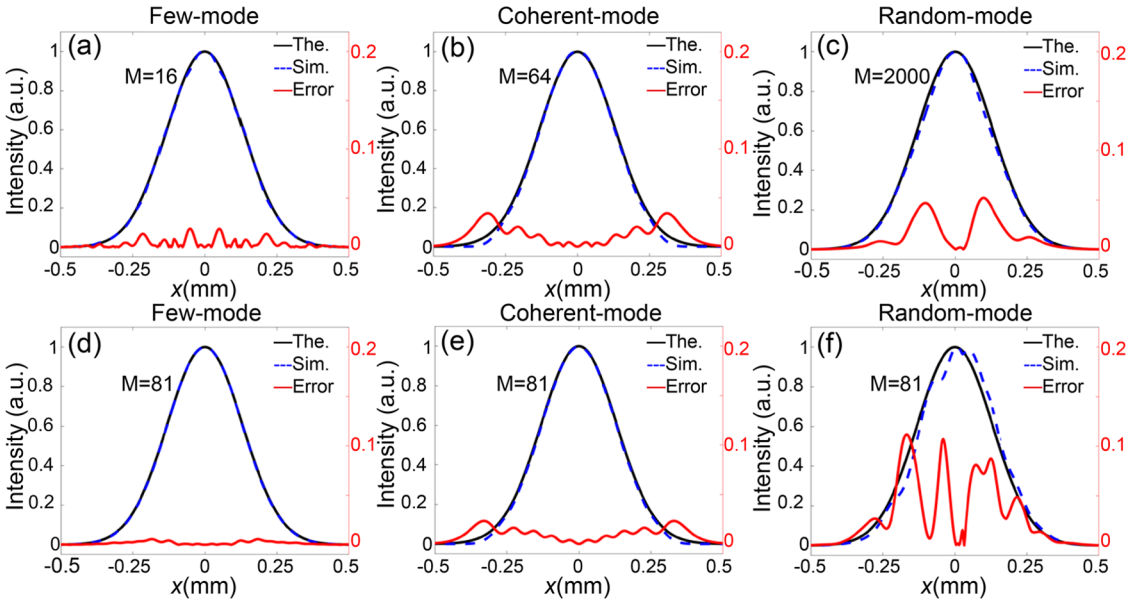

Figure 3. Comparison of intensities generated by few-mode, coherent-mode, and random-mode superposition methods. (a–c) The focal intensities of the GSM beam generated by few-mode, coherent-mode, and random-mode superposition methods. Within an error of 5%, the required modes are 16, 64, and 2000, respectively. (d–f) Comparison of GSM beam intensity errors constructed by different modal-superposition methods with the same number of modes.

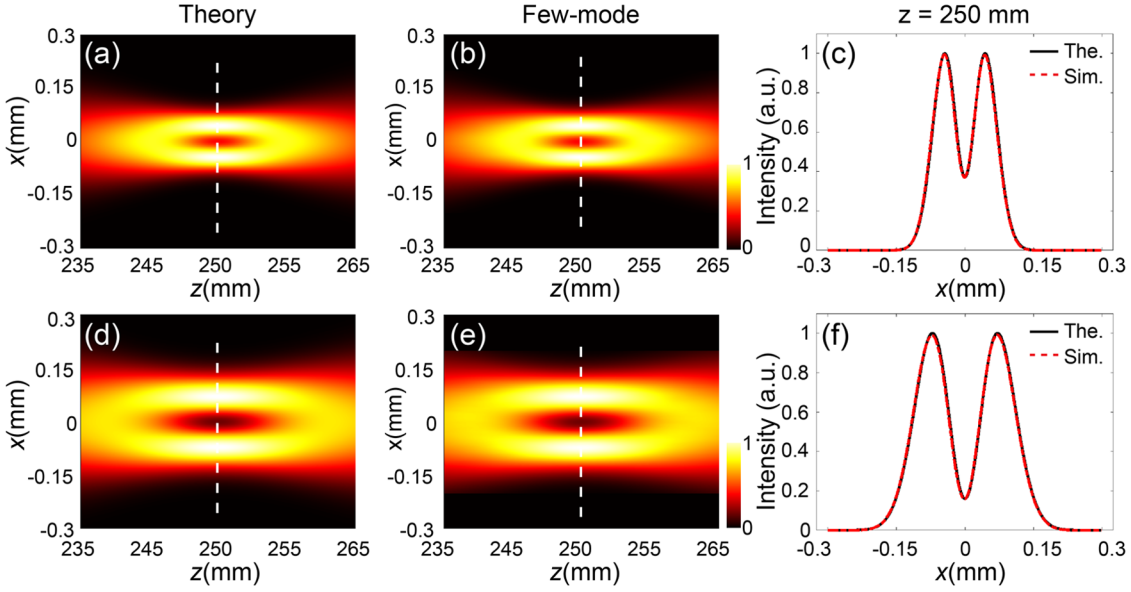

Figure 4. Generation of controllable optical cages. (a, d) are the theoretical intensity distributions of an LGCSM beam focused by a thin lens near the focal plane (x–z view) for different initial coherence widths. (b, e) are the corresponding simulation results of the optical cages generated by the few-mode superposition method. (c, f) are the fitting results of the theoretical and simulated data at z = 250 mm.

center-to-center distance between the slits is 0.4 mm. The focal interference intensity was recorded, as depicted in Figure 2i–k. The fitting curves in Figure 2l further reveal that the second-order statistics, including the intensity and the CSD distribution, of few-mode superposition in the numerical simulation and the experiment align well with those of the theoretical results.

Figure 3 compares the quality of GSM beam intensity distributions generated by few-mode, coherent-mode, and random-mode superposition. When a sufficiently large number of modes are used, all three methods are consistent with theoretical predictions. However, to enhance the efficiency of experimental or numerical simulations, a smaller number of modes is typically preferred, although a smaller number of modes may introduce errors. Using the theoretical focal field intensity as a reference, random-mode superposition requires 2000 modes to maintain an error below 5% (Figure 3c). For the same error margin, coherent-mode superposition requires 64 modes (Figure 3b), whereas few-mode superposition requires only 16 modes (Figure 3a). With the same number of modes used in modal-superposition, as shown in Figure 3d–f, the accuracy of few-mode superposition is significantly higher than that of the other two methods. To fully characterize a partially coherent source, both its intensity distribution and degree of coherence, which is essentially a normalized two-point correlation function, should be specified. Compared to

https://doi.org/10.1021/acsphotonics.4c02613
ACS Photonics 2025, 12, 2160–2168

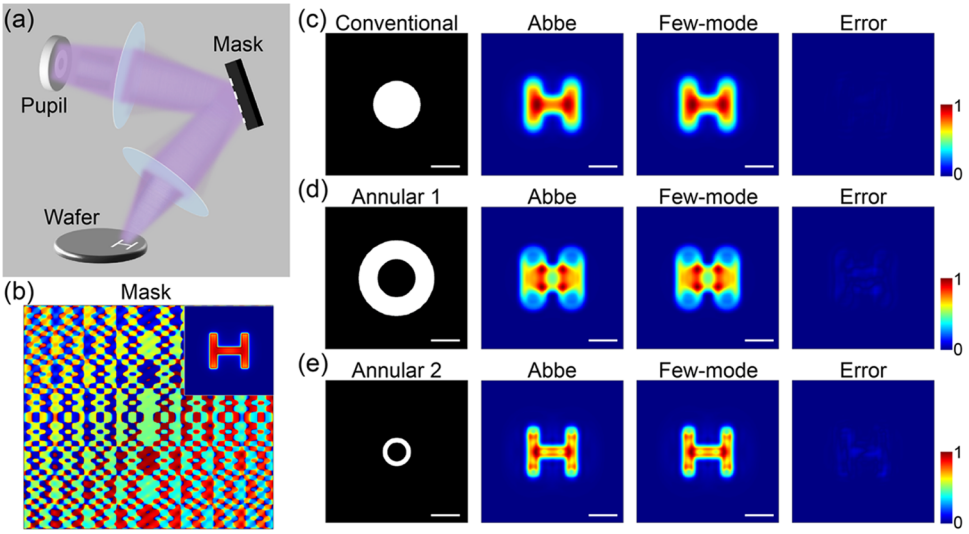

Figure 5. Predicting imaging results with few-mode superposition and Abbe method for various illuminations in lithography. (a, b) Schematic diagram of a lithography exposure system and a mask used for the generation of aerial pattern. (c–e) Predicted images on wafer for different illuminations. Scale bars in (c–e) are 30 μm.

coherent-mode and random-mode superposition methods, the few-mode superposition method provides a better reconstruction degree of coherence with the same number of modes (see Supporting Information for further details).

3.2. Generation of Optical Cage with Few-Mode Superposition. By structurally modulating the CSD functions, such as those of Laguerre–Gaussian correlated Schell-model (LGCSM) beams, PCBs exhibit interesting propagation properties. The intensity of an LGCSM beam presents a three-dimensional optical cage near the focal plane,[42,43] as shown in Figure 4. The size of this optical cage can be adjusted by modifying the initial coherence length. The CSD function of an LGCSM beam at the source plane can be expressed as[42]

$$W(\mathbf{r}_1, \mathbf{r}_2) = B_0 \exp\left(-\frac{\mathbf{r}_1^2 + \mathbf{r}_2^2}{4\sigma_0^2} - \frac{|\mathbf{r}_2 - \mathbf{r}_1|^2}{2\delta_0^2}\right) L_n^0\left[\frac{(\mathbf{r}_2 - \mathbf{r}_1)^2}{2\delta_0^2}\right] \tag{6}$$

B_0 is a constant, which was set as 1 in the following analysis. L_n^0 denotes the Laguerre polynomial of mode order n and 0. Within the validity of the paraxial approximation, the propagation of the CSD of an LGCSM beam through an ABCD optical system can be studied with the help of the extended Collins formula.[43] The intensity of the LGCSM beam on the output plane can be obtained from the CSD function as $I(\mathbf{r}_1) = W(\mathbf{r}_1, \mathbf{r}_2 = \mathbf{r}_1)$.

Figure 4a shows the theoretical intensity distributions of the LGCSM beam near the focal field, obtained through a complex quadruple integral of the four-dimensional CSD function. Here, f = 250 mm, n = 1, λ = 632 nm, σ_0 = 1 mm, and δ_0 = 0.8 mm. Given the complexity of the LGCSM beam, representing it using coherent-mode superposition is challenging, as it requires solving the eigenvalues of a Fredholm integral equation.[44] However, few-mode superposition does not require complex integral calculations, and the light intensity distribution in different planes can be determined through numerical simulation. Figure 4b shows the intensity distribution simulated by few-mode superposition, which is consistent with the theoretical results in Figure 4c. As δ_0 decreases, the optical cage gradually enlarges, as shown in Figure 4d, where the initial coherence length is set to δ_0 = 0.5 mm. The numerical simulation results using few-mode superposition are also consistent with the theoretical integral calculation results, as shown in Figure 4d–f. The controllable optical cage formed by few-mode superposition will be useful for trapping particles.

3.3. Lithography Imaging Simulation of an Aerial Pattern with Incoherent Illumination. In lithography, beam homogenization can be applied to suppress coherent noise by reducing the spatial coherence of the illumination. As shown in Figure 5a, a generic projection system is considered, including an incoherent light source, a condenser lens, a mask, an objective lens, and a resist-coated wafer.[45] To design the mask, a fully coherent Gaussian beam is assumed as the input to form the desired imaging pattern through an inverse Fourier transform algorithm. Figure 5b shows an example of the phase mask. When fully coherent light is incident on the mask, the aerial pattern on the wafer is shown in the illustration of Figure 5b (top inset).

However, considering the decoherence of the light source, the actual aerial image should be a superposition of patterns generated independently by each point on the pupil plane (a process known as the Abbe method). Modifying the pupil shape produces different images, as shown in Figure 5c–e. The focal lengths of the two lenses are 5 and 2 mm, with λ = 193 nm, and the scale bars in Figure 5c–e are 30 μm. In lithography, the illumination system can be adjusted based on the imaging results, necessitating a rapid prediction of the imaging outcomes under different incoherent illuminations. According to the Van Cittert–Zernike theorem, the incoherent light source transforms into a PCB on the mask. Therefore, the few-mode superposition method is utilized to perform the numerical simulation. The results show that the simulation with few-mode superposition is almost equivalent to the Abbe method for different illumination systems.

3.4. Low Coherent Optical Calculation with Superior Simulation Speed via Few-Mode Superposition. Regarding computation time, the few-mode superposition method demonstrates significant superiority. Calculations in a double-slit interference system and a focusing system were analyzed, as shown in Figure 6a. The sampling points in the entrance and

https://doi.org/10.1021/acsphotonics.4c02613
ACS Photonics 2025, 12, 2160–2168

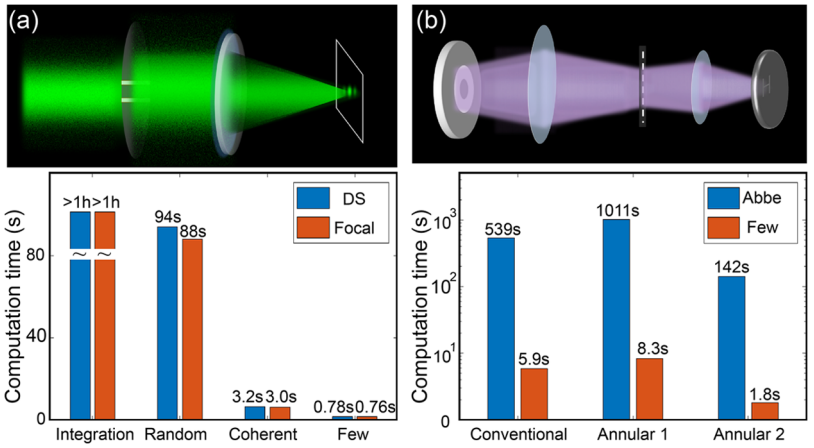

Figure 6. Comparison of time-consumption for different methods in the simulation of (a) double-slit interference and (b) lithography.

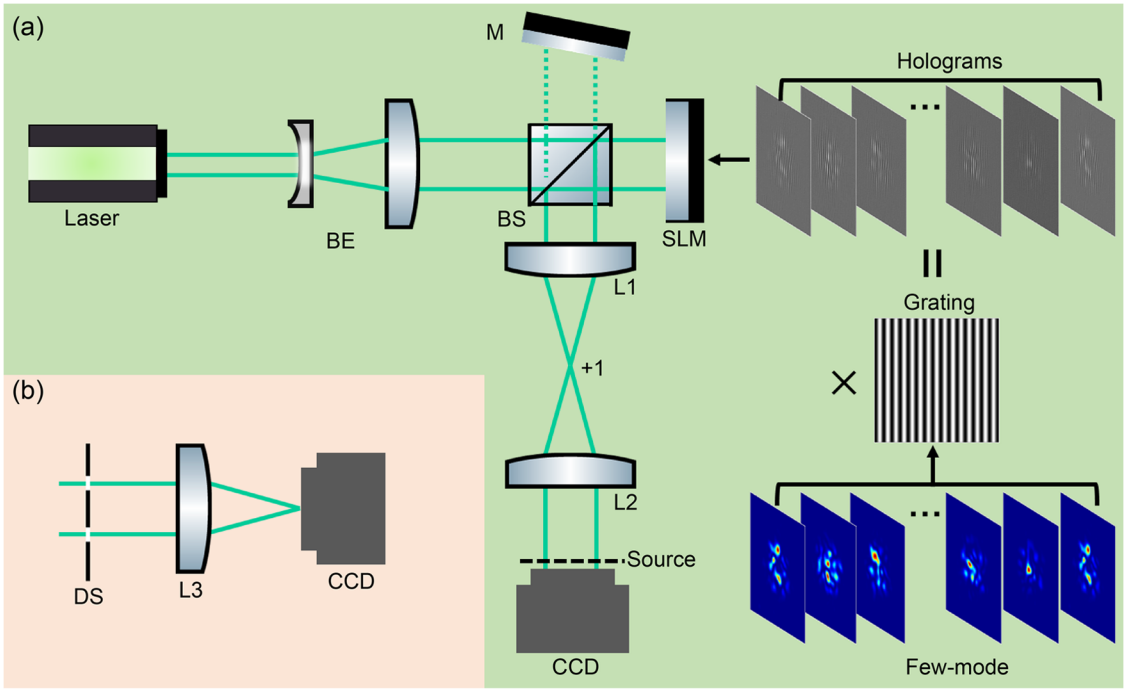

Figure 7. Schematic of the experimental setup. (a) Experimental setup for the generation of the GSM beam. BE, beam expander composed of a pinhole and a convex lens; M, reflective mirror; BS, beam splitter; SLM, spatial light modulator; L1, L2, L3, thin lenses; CCD, charge-coupled detector (ECO445). (b) Interference prediction of a GSM beam passing through a double-slit. DS: double-slit.

output fields are identical (600 × 600), with $\delta_0 = 0.4\sigma_0$. In both cases, the computational cost exceeds 1 h for the direct integration method, rendering it unsuitable for practical applications (see Supporting Information Section S1 for further details of the computational environment). For the coherent-mode and random-mode superposition methods, a large number of modes is also required to achieve the preset target accuracy, leading to a rapid increase in computation time as the number of modes increases. The computational costs for the random-mode and coherent-mode superposition methods are also shown in Figure 6a. In comparison, the proposed few-mode superposition method achieves a computation time of less than 1s, which is significantly shorter than that of the direct integration method, as well as the random-mode and coherent-mode superposition methods. This is attributed to the fact that fewer modes are required in few-mode superposition method to achieve the same precision.

In Figure 6b, the time-consumption of the Abbe method and the few-mode superposition method in lithography is compared. Due to its tedious point-by-point calculation method, the computation time of the Abbe method increases drastically with the number of calculation points on the pupil plane. This leads to a severe waste of resources, as not all mode imaging results are critical. Operating all the modes increases both the computation time and memory usage, greatly limiting its potential in practical applications. Here, the sampling points in both the entrance pupil and the wafer are the same (600 × 600), and a computational cost of approximately 539s for the Abbe method was needed. Then, the few-mode superposition method was adopted to evaluate the calculations. With 49 modes used in the few-mode superposition method, the same result can be calculated in 5.9 s. When the pupil changes, the calculation time for the Abbe method will also change accordingly. As shown in Figure 6b, approximately 1011 and

https://doi.org/10.1021/acsphotonics.4c02613
ACS Photonics 2025, 12, 2160−2168

142s are required to obtain wafer images for two types of annular illumination systems. In contrast, the few-mode superposition method consumes no more than 10 s.

4. DISCUSSION AND CONCLUSIONS

The proposed few-mode superposition method enhances the modal-superposition calculation of partially coherent fields. First, the few-mode superposition method for the experimental generation of PCBs enables rapid generation of partially coherent fields with various CSD distributions. Second, it offers greater flexibility compared to other modal-superposition methods, without sacrificing accuracy or efficiency. Third, the method demonstrates strong universality in predicting the propagation of PCBs with nonconventional CSD functions. It can be applied to lithography imaging prediction of incoherent light sources. Notably, the proposed method facilitates faster calculation of PCBs compared to other modal-superposition methods. In conclusion, the few-mode superposition method holds significant promise for efficient PCB generation, optical proximity correction in lithography, and fast simulations of optical processes with partially coherent illumination, such as synchrotron radiation sources and X-rays.

Furthermore, the feasibility of using an iterative method to calculate the modes in the few-mode superposition method is confirmed by reconstructing the intensity of the beam passing through the scatterer. As the degree of coherence length decreases, more modes are required for iteration, increasing the memory and computational time requirements. Therefore, for numerical simulations of low coherence or incoherent light fields, subregions can be utilized for iteration. The entire light field can be spliced and integrated to obtain comprehensive light field information. In practice, the number of modes for iteration and the intensity acquisition scheme can be selected based on specific requirements.

5. METHODS

5.1. Experimental Setup for PCB Generation with Few-Mode Superposition. The experimental setup is illustrated in Figure 7 The beam from a diode-pumped solid-state laser source was expanded into a near-plane wave using a beam expander and subsequently illuminated a spatial light modulator (SLM). The holograms shown in Figure 7 were loaded onto the SLM to modulate the amplitude and phase distribution of the incident beam. The light field reflected from the SLM passed through the beam splitter (BS) and a 4*f* optical system composed of lenses L1 and L2 (each with a focal length of 250 mm). A filter was positioned at the back focal plane of L1 to select beams with a diffraction order of +1, which were then collected at the output plane of the 4*f* system using a CCD. The output plane of the 4*f* system (dashed line in Figure 7a) was used as the source plane, and a camera recorded the source intensity by superimposing the intensities from all the holograms. A mirror was added above the BS to measure the CSD using off-axis holography.[41] The accuracy of the generated beam was further validated through a double-slit interference experiment. The double-slit was positioned behind the source plane, and the camera was placed at the focal plane of L3 (f = 250 mm), as depicted in Figure 7b.

5.2. Few-Mode Iterative Method. To calculate the modes of few-mode superposition, an iteration algorithm was used. The partially coherent light field can be regarded as an incoherent modal superposition of multiple electric fields, thus the CSD can be decomposed as $W(\mathbf{r}_1, \mathbf{r}_2) = \sum_m E_m^*(\mathbf{r}_1)E_m(\mathbf{r}_2)$. After propagation, the intensity $I_0(\mathbf{k})$ will be the incoherent superposition of the diffraction intensities of all the modes, denoted as $I_0(\mathbf{k}) = \sum_m \psi_m(\mathbf{k})\psi_m^*(\mathbf{k})$. Each $\psi_m(\mathbf{k})$ represents the diffraction field of $E_m(\mathbf{r})$.

Then, a typical diffraction imaging process was simulated to calculate the modes representing the PCB:

(1) First, the number of modes in the source plane is set to M, and an initial guess was made for a series of $E_m^i(\mathbf{r})$. The distribution of the diffraction field $\psi_m(\mathbf{k})$ (e.g., at the focal plane) can be determined by

$$\psi_m^i(\mathbf{k}) = \mathcal{F}\{E_m^i(\mathbf{r})\cdot O(\mathbf{r})\} \tag{7}$$

where $\mathbf{r}$ is the coordinate on the source plane and $\mathbf{k}$ is the coordinate on the output plane. $O(\mathbf{r})$ denotes a known object (a resolution test chart).

(2) The diffraction field was further updated using the recorded intensity as

$$\psi_m^{i'}(\mathbf{k}) = \frac{\sqrt{I_0(\mathbf{k})}}{\sqrt{\sum_{m=1}^{M}\psi_m^i(\mathbf{k})\psi_m^{*i}(\mathbf{k})}}\psi_n^i(\mathbf{k}) \tag{8}$$

"m" represents the m-th mode, whose total number is M, and "i" is the i-th iteration.

$$E_m^{i+1}(\mathbf{r}) = E_m^i(\mathbf{r}) + \beta\frac{O^*(\mathbf{r})}{|O(\mathbf{r})|^2_{\max}}[\Phi'^i_m(\mathbf{r}) - \Phi_m^i(\mathbf{r})] \tag{9}$$

where $\Phi'^i_m(\boldsymbol{\rho}) = \mathcal{F}^{-1}\{\psi_m^{i'}(\mathbf{k})\}$. β is an update factor, set to 0.8 in this work. $\mathcal{F}$ and $\mathcal{F}^{-1}$ represent forward and backward diffraction propagation, respectively.

(4) To generate additional constraints for the multimode iteration algorithms, overlap-scanning was performed to obtain multiple intensities. For each scan position, steps (1−3) were repeated.

(5) Steps (1−4) were repeated until the iterative error between the recovered intensity $I_r(\mathbf{k}) = \sum_n \psi_m^i(\mathbf{k})\psi_m^{i*}(\mathbf{k})$ and the theoretical intensity $I_0(\mathbf{k})$ is less than a predetermined threshold. Here, $E_m(\mathbf{r})$ was reconstructed after 20 iterations, and the cross-spectral density was reconstructed based on $W(\mathbf{r}_1, \mathbf{r}_2) = \sum_{m=1}^{M} E_m^*(\mathbf{r}_1)E_m(\mathbf{r}_2)$.

■ ASSOCIATED CONTENT

Data Availability Statement

The data and codes supporting this study are available upon reasonable request from the corresponding author.

Supporting Information

The Supporting Information is available free of charge at https://pubs.acs.org/doi/10.1021/acsphotonics.4c02613.

Computational environment (Section S1); generating the degree of coherence of PCBs using modal-superposition (Section S2) (PDF)

■ AUTHOR INFORMATION

Corresponding Authors

Xingyuan Lu − *School of Physical Science and Technology, Jiangsu Key Laboratory of Frontier Material Physics and Devices, Soochow University, Suzhou 215006, China*; Email: xylu@suda.edu.cn

https://doi.org/10.1021/acsphotonics.4c02613
ACS Photonics 2025, 12, 2160−2168

Chengliang Zhao − *School of Physical Science and Technology, Jiangsu Key Laboratory of Frontier Material Physics and Devices, Soochow University, Suzhou 215006, China;* orcid.org/0000-0003-3703-889X; Email: zhaochengliang@suda.edu.cn

Authors

Zhuoyi Wang − *School of Physical Science and Technology, Jiangsu Key Laboratory of Frontier Material Physics and Devices, Soochow University, Suzhou 215006, China*

Hao Zhang − *School of Physics and Engineering, Henan University of Science and Technology, Luoyang 471023, China*

Junan Zhu − *School of Physical Science and Technology, Jiangsu Key Laboratory of Frontier Material Physics and Devices, Soochow University, Suzhou 215006, China*

Xiaotan Lu − *School of Physical Science and Technology, Jiangsu Key Laboratory of Frontier Material Physics and Devices, Soochow University, Suzhou 215006, China*

Yifeng Shao − *Imaging Physics Department, Applied Science Faculty, Delft University of Technology, Delft 2628 CJ, The Netherlands*

H. Paul Urbach − *Imaging Physics Department, Applied Science Faculty, Delft University of Technology, Delft 2628 CJ, The Netherlands*

Qiwen Zhan − *School of Optical-Electrical and Computer Engineering, University of Shanghai for Science and Technology, Shanghai 200093, China*

Yangjian Cai − *Shandong Provincial Engineering and Technical Center of Light Manipulations & Shandong Provincial Key Laboratory of Optics and Photonic Device, School of Physics and Electronics, Shandong Normal University, Jinan 250358, China; Joint Research Center of Light Manipulation Science and Photonic Integrated Chip, East China Normal University, Shanghai 200241, China;* orcid.org/0000-0003-3440-7709

Complete contact information is available at: https://pubs.acs.org/10.1021/acsphotonics.4c02613

Author Contributions

Z.W., X.L., H.Z., J.Z., X.L., and Q.Z. proposed the original idea and performed the theoretical analysis. Z.W., Y.S., H.P.U., and X.L.: Performed the experiments, data analysis and contributed to the development of the measurement method. X.L., C.Z., Q.Z., and Y.C.: Supervised the project. All the authors contributed to the data analysis and writing of the manuscript.

Notes

The authors declare no competing financial interest.

■ ACKNOWLEDGMENTS

This work was supported by the National Key Research and Development Program of China (No. 2022YFA1404800), National Natural Science Foundation of China (No. 12174280, No. 12204340, No. 12192254, No. 12404343, No. 92250304, No. 12434012, No. W2441005), Priority Academic Program Development of Jiangsu Higher Education Institutions, and Postgraduate Research & Practice Innovation Program of Jiangsu Province (KYCX24_3287).

■ REFERENCES

(1) Maiman, T. Stimulated emission of radiation in ruby. *Nature* **1960**, *187*, 493−494.
(2) Forbes, A. Structured light from lasers. *Laser Photonics Rev.* **2019**, *13*, No. 1900140.
(3) Bartels, R. A.; Paul, A.; Green, H.; et al. Generation of spatially coherent light at extreme ultraviolet wavelengths. *Science* **2002**, *297*, 376−378.
(4) Peng, Y.; Choi, S.; Kim, J.; Wetzstein, G. Speckle-free holography with partially coherent light sources and camera-in-the-loop calibration. *Sci. Adv.* **2021**, *7*, No. 5040.
(5) Chen, X.; Kandel, M.; Hu, C.; et al. Wolf phase tomography (WPT) of transparent structures using partially coherent illumination. *Light Sci. Appl.* **2020**, *9*, No. 142.
(6) Tong, X.; Xu, R.; Xu, P.; et al. Harnessing the magic of light: spatial coherence instructed swin transformer for universal holographic imaging. *Adv. Photonics* **2023**, *5*, No. 066003.
(7) Dong, B.; Brückerhoff-Plückelmann, F.; Meyer, L.; et al. Partial coherence enhances parallelized photonic computing. *Nature* **2024**, *632*, 55−62.
(8) Clark, J.; Huang, X.; Harder, R.; Robinson, I. High-resolution three-dimensional partially coherent diffraction imaging. *Nat. Commun.* **2012**, *3*, No. 993.
(9) Redding, B.; Choma, M.; Cao, H. Speckle-free laser imaging using random laser illumination. *Nat. Photonics* **2012**, *6*, 355−359.
(10) Kip, D.; Soljacic, M.; Segev, M.; et al. Modulation Instability and Pattern Formation in Spatially Incoherent Light Beams. *Science* **2000**, *290*, 495−498.
(11) Wang, F.; Liu, X.; Cai, Y. Propagation of partially coherent beam in turbulent atmosphere: a review (invited review). *Prog. Electromagn. Res.* **2015**, *150*, 123−143.
(12) Lu, X.; Wang, Z.; Zhan, Q.; et al. Coherence entropy during propagation through complex media. *Adv. Photonics* **2024**, *6*, No. 046002.
(13) Thibault, P.; Menzel, A. Reconstructing state mixtures from diffraction measurements. *Nature* **2013**, *494*, 68−71.
(14) Whitehead, L. W.; Williams, G.; Quiney, H.; et al. Diffractive imaging using partially coherent x rays. *Phys. Rev. Lett.* **2009**, *103*, No. 243902.
(15) Chen, Z.; Odstrcil, M.; Jiang, Y.; et al. Mixed-state electron ptychography enables sub-angstrom resolution imaging with picometer precision at low dose. *Nat. Commun.* **2020**, *11*, No. 2994.
(16) Burdet, N.; Shi, X.; Parks, D.; et al. Evaluation of partial coherence correction in X-ray ptychography. *Opt. Express* **2015**, *23*, 5452−5467.
(17) Abbey, B.; Whitehead, L.; Quiney, H.; et al. Lensless imaging using broadband X-ray sources. *Nat. Photonics* **2011**, *5*, 420−424.
(18) Ma, X.; Arce, G. Binary mask optimization for inverse lithography with partially coherent illumination. *J. Opt. Soc. Am. A* **2008**, *25*, 2960−2970.
(19) Li, Z.; Dong, L.; Ma, X.; Wei, Y. Decomposition-learning-based thick-mask model for partially coherent lithography system. *Opt. Express* **2023**, *31*, 20321−20337.
(20) Wolf, E. *Introduction to the Theory of Coherence and Polarization of Light*; Cambridge University Press, 2007.
(21) Gori, F. Collett-Wolf sources and multimode lasers. *Opt. Commun.* **1980**, *34*, 301−305.
(22) Gori, F.; Santarsiero, M. Devising genuine spatial correlation functions. *Opt. Lett.* **2007**, *32*, 3531−3533.
(23) Barré, N.; Jesacher, A. Holographic beam shaping of partially coherent light. *Opt. Lett.* **2022**, *47*, 425−428.
(24) Lu, X.; Wang, Z.; Zhao, C.; et al. Four-dimensional experimental characterization of partially coherent light using incoherent modal decomposition. *Nanophotonics* **2023**, *12*, 3463−3470.
(25) Waller, L.; Situ, G.; Fleischer, J. Phase-space measurement and coherence synthesis of optical beams. *Nat. Photonics* **2012**, *6*, 474−479.
(26) Mack, C. *Fundamental Principles of Optical Lithography: The Science of Microfabrication*; John Wiley & Sons, 2007.

(27) Yu, J.; Zhu, X.; Wang, F.; et al. Research progress on manipulating spatial coherence structure of light beam and its applications. *Prog. Quantum Electron.* **2023**, *91*−*92*, No. 100486.
(28) Wang, F.; Lv, H.; Chen, Y.; et al. Three modal decompositions of Gaussian Schell-model sources: comparative analysis. *Opt. Express* **2021**, *29*, 29676−29689.
(29) Liu, X.; Chen, Q.; Zeng, J.; et al. Measurement of optical coherence structures of random optical fields using generalized Arago spot experiment. *Opto. Electron. Sci.* **2023**, *2*, No. 220024.
(30) Li, Z.; Dong, L.; Ma, X. Fast source mask co-optimization method for high-NA EUV lithography. *Opt. Electron. Adv.* **2024**, *7*, No. 230235.
(31) Hyde, M. W. Stochastic complex transmittance screens for synthesizing general partially coherent sources. *J. Opt. Soc. Am. A* **2020**, *37*, 257−264.
(32) Liu, L.; Liu, W.; Wang, F.; et al. Spatial coherence manipulation on the disorder-engineered statistical photonic platform. *Nano Lett.* **2022**, *22*, 6342−6349.
(33) Liu, L.; Liu, W.; Wang, F.; et al. Ultra-robust informational metasurfaces based on spatial coherence structures engineering. *Light Sci. Appl.* **2024**, *13*, No. 131.
(34) Roques-Carmes, C.; Fan, S.; Miller, D. Measuring, processing, and generating partially coherent light with self-configuring optics. *Light Sci. Appl.* **2024**, *13*, No. 260.
(35) Zhu, X.; Yu, J.; Chen, Y.; et al. Generation of Stochastic Structured Light Beams with Controllable Beam Parameters. *ACS Photonics* **2023**, *10*, 2272−2279.
(36) Wang, H.; Peng, X.; Zhang, H.; et al. Experimental synthesis of partially coherent beam with controllable twist phase and measuring its orbital angular momentum. *Nanophotonics* **2022**, *11*, 689−696.
(37) Xu, H.; Zhu, Z.; Li, X.; et al. Wave-optics simulation software for synchrotron radiation from 4th generation storage rings based on a coherent modes model. *Opt. Express* **2022**, *30*, 7625−7635.
(38) Dai, S.; Zheng, X.; Zhao, S. Designing diffractive optical elements for shaping partially coherent beams by proximity correction. *Opt. Express* **2023**, *31*, 14464−14472.
(39) Steinwart, I.; Scovel, C. Mercer's theorem on general domains: On the interaction between measures, kernels, and RKHSs. *Constr. Approximation* **2012**, *35*, 363−417.
(40) Wolf, E.; Collett, E. Partially coherent sources which produce the same far-field intensity distribution as a laser. *Opt. Commun.* **1978**, *25*, 293−296.
(41) Li, W.; Liu, Y.; Chen, Y.; et al. Fast measurement of coherence−orbital angular momentum matrices of random light beams using off-axis holography and coordinate transformation. *Opt. Lett.* **2024**, *49*, 1173−1176.
(42) Mei, Z.; Korotkova, O. Random sources generating ring-shaped beams. *Opt. Lett.* **2013**, *38*, 91−93.
(43) Chen, Y.; Cai, Y. Generation of a controllable optical cage by focusing a Laguerre−Gaussian correlated Schell-model beam. *Opt. Lett.* **2014**, *39*, 2549−2552.
(44) Yuan, D.; Zhang, X. An overview of numerical methods for the first kind Fredholm integral equation. *SN Appl. Sci.* **2019**, *1*, No. 1178.
(45) Bakshi, V. *EUV Lithography*; SPIE Press, 2009.

https://doi.org/10.1021/acsphotonics.4c02613
ACS Photonics 2025, 12, 2160−2168